NeuroImage 49 (2010) 1432–1445

Contents lists available at ScienceDirect

NeuroImage

journal homepage: www.elsevier.com/locate/ynimg

# The oscillating brain: Complex and reliable

Xi-Nian Zuo [a], Adriana Di Martino [a], Clare Kelly [a], Zarrar E. Shehzad [a], Dylan G. Gee [a], Donald F. Klein [a,b,d], F. Xavier Castellanos [a,b], Bharat B. Biswal [b,c,*], Michael P. Milham [a,*]

[a] Phyllis Green and Randolph Cōwen Institute for Pediatric Neuroscience at the New York University Child Study Center, New York, NY, USA
[b] Nathan Kline Institute for Psychiatric Research, Orangeburg, NY, USA
[c] Department of Radiology, University of Medicine and Dentistry of New Jersey, Newark, NJ, USA
[d] Department of Psychiatry, Professor Emeritus, College of Physicians and Surgeons, Columbia University, New York, NY, USA

ARTICLE INFO

*Article history:*
Received 17 July 2009
Revised 18 August 2009
Accepted 17 September 2009
Available online 24 September 2009

ABSTRACT

The human brain is a complex dynamic system capable of generating a multitude of oscillatory waves in support of brain function. Using fMRI, we examined the amplitude of spontaneous low-frequency oscillations (LFO) observed in the human resting brain and the test–retest reliability of relevant amplitude measures. We confirmed prior reports that gray matter exhibits higher LFO amplitude than white matter. Within gray matter, the largest amplitudes appeared along mid-brain structures associated with the "default-mode" network. Additionally, we found that high-amplitude LFO activity in specific brain regions was reliable across time. Furthermore, parcellation-based results revealed significant and highly reliable ranking orders of LFO amplitudes among anatomical parcellation units. Detailed examination of individual low frequency bands showed distinct spatial profiles. Intriguingly, LFO amplitudes in the slow-4 (0.027–0.073 Hz) band, as defined by Buzsáki et al., were most robust in the basal ganglia, as has been found in spontaneous electrophysiological recordings in the awake rat. These results suggest that amplitude measures of LFO can contribute to further between-group characterization of existing and future "resting-state" fMRI datasets.


## Introduction

The human brain is a complex dynamical system generating a multitude of oscillatory waves. To characterize the diverse oscillatory array, Buzsáki and colleagues proposed a hierarchical organization of 10 frequency bands they termed 'oscillation classes,' extending from 0.02 to 600 Hz (Buzsáki and Draguhn, 2004; Penttonen, 2003). They noted that oscillations within specific classes have been linked with a variety of neural processes, including input selection, plasticity, binding, and consolidation (Buzsáki and Draguhn, 2004) as well as cognitive functions including salience detection, emotional regulation, attention and memory (Knyazev, 2007). Recently, low-frequency oscillations (LFO; typically defined as frequencies <0.1 Hz) have gained increased attention based on observations using fMRI approaches and direct current coupled electroencephalographic scalp recordings (Demanuele et al., 2007; Fox and Raichle, 2007). Using these modalities, researchers have consistently identified coherent spontaneous low-frequency fluctuations in the 0.01–0.1 Hz range during both resting and active-task conditions that are thought to reflect cyclic modulation of gross cortical excitability and long distance neuronal synchronization (Balduzzi et al., 2008; Buzsáki and Draguhn, 2004; Vanhatalo et al., 2004).

Despite the increased appreciation of spontaneous LFO in BOLD fMRI resting state data (Fox and Raichle, 2007), the properties and regional characteristics of spontaneous LFO rarely have been examined directly. Instead, most resting state fMRI studies have focused on mapping the spatial distribution of temporal correlations among these spontaneous fluctuations. This is commonly referred to as "resting-state functional connectivity" (RSFC). RSFC approaches generate highly detailed maps of complex functional systems (Di Martino et al., 2008b; Fox and Raichle, 2007; Margulies et al., 2007), which have been shown to be both reliable over time (Deuker et al., 2009; Shehzad et al., 2009) and reproducible across different data sets (He et al., 2009). Using these approaches, numerous clinical studies have already identified a variety of abnormalities in RSFC thought to reflect pathophysiological processes (Broyd et al., 2009; Greicius, 2008; Seeley et al., 2009). Between-subject differences in RSFC measures also correlate strongly with individual traits and behavioral characteristics (Di Martino et al., 2009; Fox et al., 2007; Hampson et al., 2006; Hesselmann et al., 2008; Kelly et al., 2008). Overall, RSFC has proven to be a powerful and efficient tool for neuroimaging studies of brain physiology and pathophysiology.

Although infrequently examined, other aspects of LFO observed during rest may also prove informative. Of particular interest to the present work is LFO amplitude information, which is commonly overlooked as a potential index of spontaneous fluctuations during

* Corresponding authors. M.P. Milham is to be contacted at 215 Lexington Avenue 14th Floor, New York, NY 10016, USA. Fax: +1 212 263 4675. B.B. Biswal, Suite 575, 30 Bergen Street, Newark, NJ 07103, USA. Fax: +1 973 972 7363.
*E-mail addresses:* bbiswal@yahoo.com (B.B. Biswal), michael.milham@nyumc.org (M.P. Milham).

1053-8119/$ – see front matter © 2009 Elsevier Inc. All rights reserved.
doi:10.1016/j.neuroimage.2009.09.037

rest. The few fMRI studies that have directly examined variations in LFO amplitudes have found meaningful differences among brain regions and among clinical populations. Around 15 years ago, the first studies reported regional differences in LFO amplitude (Biswal et al., 1995; Jezzard et al., 1993). Specifically, they observed amplitudes that were higher in gray matter than in white matter. Kiviniemi et al. (2003) found distinct LFO patterns across visual, auditory and sensorimotor regions; LFO in visual regions had the highest magnitude. Several recent studies located the highest LFO amplitudes within posterior structures along the brain's midline (Zang et al., 2007; Zou et al. , 2008, 2009). The feasibility of detecting regional differences in LFO amplitudes is also supported by a recent computational simulation, in which the highest oscillatory amplitudes emerged in cingulate and medial prefrontal cortices (Ghosh et al., 2008).

Beyond within-subject regional differences, recent work suggests that LFO amplitudes differ in clinical populations compared to healthy controls. Specifically, children with attention-deficit/hyperactivity disorder (ADHD) showed increased LFO amplitude in anterior cingulate and sensorimotor cortices and decreased LFO amplitude in inferior frontal cortex (Zang et al., 2007). More recently, patients with mesial temporal lobe epilepsy (Zhang et al., 2008) exhibited marked increases in LFO amplitude within the right precentral gyrus in addition to decreases in amplitude within the "default-mode" network (Raichle et al., 2001), particularly in the posterior cingulate, medial frontal and anterior cingulate cortices. Although these reports have yet to be replicated, the detection of between-group differences in LFO amplitude suggests that these measures may reflect stable trait properties.

While these studies imply that LFO amplitudes may represent a potentially meaningful and stable property of the human brain, several physiological and neural factors also can impact LFO amplitudes. Biswal et al. (1997) observed that LFO amplitudes are sensitive to carbon dioxide ($CO_2$) levels (i.e., room air vs. 5% $CO_2$), with amplitudes suppressed by hypercapnea. Similarly, Wise et al. (2004) demonstrated that a component of low frequency BOLD fluctuations could reflect carbon dioxide-induced changes in cerebral blood flow. Several studies have demonstrated task-related modulation of LFO amplitude measures. During working memory task performance, regions of the "default-mode" network (e.g., anterior and posterior midline areas) exhibited task-related reductions in LFO amplitude (Fransson, 2006). Duff et al. (2008) also demonstrated task-related reductions in LFO amplitude measures, affecting both task-activated regions (e.g., supplementary motor area, motor cortices) and task-deactivated regions (e.g., posterior cingulate cortex). Some studies suggest that the specific instructions (e.g., rest with eyes open vs. rest with eyes closed) impact LFO amplitude in regions such as visual cortex (McAvoy et al., 2008; Yang et al., 2007). Similarly, LFO amplitude is sensitive to arousal level. Sleep produces stage-dependent alterations in amplitude patterns (Fukunaga et al., 2008; Horovitz et al., 2008; Picchioni et al., 2008). Degree of anesthesia and sedation also affect LFO amplitude (Kiviniemi et al., 2000; Kiviniemi et al., 2005). Finally, an increasing number of studies have drawn attention to the potential artifactual contributions of cardiac and respiratory-related processes to LFO amplitude measures (Bianciardi et al., 2009; Birn et al., 2006; Chang et al., 2009; van Buuren et al., 2009; Yan et al., 2009). In summary, the various physiological and state factors that can impact regional measures of LFO amplitude raise concerns regarding test–retest reliability.

The present work provides a comprehensive examination of two Fast Fourier Transform (FFT)-based indices of LFO amplitude: (1) amplitude of low frequency fluctuations (ALFF) (Zang et al., 2007) and (2) fractional amplitude of low frequency fluctuations (fALFF) (Zou et al., 2008). ALFF is defined as the total power within the frequency range between 0.01 and 0.1 Hz. Although ALFF is effective at detecting LFO fluctuations, the fluctuations detected can extend over 0.1 Hz, particularly near major vessels (Zou et al., 2008), which are characterized by widespread oscillations across both low and high frequencies. In contrast, fALFF is defined as the total power within the low-frequency range (0.01–0.1 Hz) divided by the total power in the entire detectable frequency range, which is determined by sampling rate and duration. As a normalized index of ALFF, fALFF can provide a more specific measure of low-frequency oscillatory phenomena.

For both ALFF and fALFF, we (1) characterized their spatial distributions and (2) investigated their test–retest reliabilities. Prior work has consistently demonstrated gray vs. white matter distinctions for ALFF and fALFF measures, with low-frequency fluctuations being more detectable within gray matter (Jezzard et al., 1993; Biswal et al., 1995; Zang et al., 2007; Zou et al., 2008). However, regional differences among gray matter regions have not been examined in detail. Furthermore, ALFF and fALFF have yet to be directly compared. Second, the increasing application of LFO amplitude measures in clinical studies requires that the reliability of these measures be addressed directly. We conducted our analyses using a previously collected fMRI dataset (Shehzad et al., 2009), comprising 26 participants scanned on three different occasions, which allowed us to assess both inter-session (5–16 months apart) and intra-session (<1 h apart) reliability.

Finally, while the RSFC literature has typically focused on all fluctuations below 0.1 Hz (Cordes et al., 2001), specific frequency bands within the LFO range may contribute differentially to RSFC (Salvador et al., 2008). For example, Buzsáki and colleagues noted that neuronal oscillation classes are arrayed linearly when plotted on the natural logarithmic scale (Buzsáki and Draguhn, 2004; Penttonen, 2003). They asserted that this regularity and much empirical data at higher frequencies suggest that independent frequency bands are generated by distinct oscillators, each with specific properties and physiological functions. However, with a few exceptions (Cordes et al., 2001; Salvador et al., 2007, 2008), fMRI studies rarely consider divisions of the power spectrum beyond the most basic division of low (<0.1 Hz) and high (>0.1 Hz) frequencies. Accordingly, in our analyses, we incorporate the Buzsáki framework, which allows us to differentiate four frequency bands instead of two.

## Methods

### *Participants and data acquisition*

We used a dataset comprising 26 participants (mean age 20.5 ± 4.8 years, 11 males) who were scanned three times as part of an earlier study that examined the test–retest reliability of RSFC (Shehzad et al., 2009). All participants were without a history of psychiatric or neurological illness as confirmed by psychiatric clinical assessment. Informed consent was obtained prior to participation. Data collection was carried out according to protocols approved by the institutional review boards of New York University (NYU) and the NYU School of Medicine.

Three resting-state scans were obtained for each participant using a Siemens Allegra 3.0-Tesla scanner. Each scan consisted of 197 contiguous EPI functional volumes (TR = 2000 ms; TE = 25 ms; flip angle = 90°, 39 slices, matrix = 64 × 64; FOV = 192 mm; acquisition voxel size = 3 × 3 × 3 mm). Scans 2 and 3 were conducted in a single-scan session, 45 min apart, and were 5–16 months (mean 11 ± 4) after scan 1. All individuals were asked to relax and remain still with eyes open during the scan. For spatial normalization and localization, a high-resolution T1-weighted magnetization prepared gradient echo sequence was also obtained (MPRAGE, TR = 2500 ms; TE = 4.35 ms; TI = 900 ms; flip angle = 8°; 176 slices; FOV=256 mm).

### *Image preprocessing*

Preliminary data preprocessing was carried out using both FMRIB Software Library (FSL: *http://www.fmrib.ox.ac.uk/fsl*, version 4.1) and Analysis of Functional NeuroImaging (AFNI: *http://afni.nimh.nih.gov/*

*afni*, version 2008_07_18_1710). Image preprocessing was mostly consistent with previous studies on ALFF (Zang et al., 2007; Zou et al., 2008) and included (1) slice time correction for interleaved acquisitions using Sinc interpolation with a Hanning windowing kernel (FSL command: *slicetimer*), (2) 3D motion correction via a robust and accurate intra-modal volume linear registration (FSL command: *mcflirt*), (3) despiking of extreme time series outliers using a hyperbolic tangent function (AFNI command: *3dDespike*), (4) 4D normalization of the entire data set by a single scaling factor (i.e., all volumes scaled by the same amount) to ensure a valid high-level analysis (FSL command: *fslmaths*), (5) spatial smoothing via a Gaussian kernel with FWHM = 6 mm (FSL command: *fslmaths*), (6) removal of linear trends (AFNI command: *3dTcat*), and (7) estimation of a nonlinear transformation from individual functional space into MNI152 space (FSL commands: *flirt* and *fnirt*). Of note, the 4D data normalization in step 4 differs from the so-called "global signal normalization" frequently used in the RSFC literature, which forces each 3D volume to have a same mean value (Fox et al., 2009; Murphy et al., 2009). No temporal filtering was implemented during preprocessing. This assures that the entire frequency band below the Nyquist frequency (0.25 Hz) can be examined in subsequent analyses of LFO amplitude.

### *Computing ALFF and fALFF*

For each scan and each participant, we performed ALFF and fractional ALFF (fALFF) analyses to identify those voxels with significantly detectable LFO amplitude (ALFF) or proportion of LFO amplitude (fALFF). For a timeseries x(t), ALFF is calculated as the sum of amplitudes within a specific low frequency range (in equation (1): 0.01–0.1 Hz). Fractional ALFF is the ALFF of given frequency band expressed as a fraction of the sum of amplitudes across the entire frequency range detectable in a given signal. The two measures reflect different aspects of LFO amplitude: ALFF indexes the strength or intensity of LFO, while fALFF represents the relative contribution of specific LFO to the whole detectable frequency range. In fact, as shown in equation (2), fALFF can be regarded as a normalized ALFF, using the total energy over the detectable frequency range. In practice, the total energy of entire signals may be different across brain regions (e.g., voxels), which can lead fALFF to differ from ALFF in some regions more than others. The ALFF measure is analogous to Resting-State Fluctuations Amplitude (RSFA) (Kannurpatti and Biswal, 2008), which is a time-domain LFO amplitude measure calculated as the standard deviation of low-pass filtered (<0.1 Hz) "resting state" timeseries. However, computing measures of LFO amplitude in the frequency domain has the advantage of offering the ability to simultaneously examine specific bands within the LFO frequency range.

$$x(t) = \sum_{k=1}^{N} [a_k \cos(2\pi f_k t) + b_k \sin(2\pi f_k t)] \tag{0}$$

$$ALFF = \sum_{k:f_k \in [0.01,0.1]} \sqrt{\frac{a_k^2(f) + b_k^2(f)}{N}} \tag{1}$$

$$fALFF = \sum_{k:f_k \in [0.01,0.1]} \sqrt{\frac{a_k^2(f_k) + b_k^2(f_k)}{N}} \Big/ \sum_{k=1}^{N} \sqrt{\frac{a_k^2(f_k) + b_k^2(f_k)}{N}} \tag{2}$$

We first computed ALFF and fALFF for every voxel in the brain. Prior to subsequent analyses, subject-level voxel-wise ALFF maps were standardized into subject-level *Z*-score maps (i.e., by subtracting the mean voxel-wise ALFF obtained for the entire brain, and then dividing by the standard deviation). The same *Z*-transform was applied to subject-level fALFF maps. The standardized ALFF and fALFF can improve the subsequent statistical analyses on group-level LFO amplitude measures and their test–retest reliability (see Supplementary Text "The Usage of Standardized LFO Amplitude Measures"). Fig. 1 provides a schematic of the computation procedure. We consider the mean LFO amplitude (ALFF and fALFF) for the entire brain to be the baseline of LFO amplitude (ALFF and fALFF).

### *Spatial normalization*

The nonlinear transformation from preprocessing step 7 was used for two spatial normalization procedures. First, to perform group statistical analyses, we converted all individual *Z*-score maps to MNI152 standard space with 2×2×2 mm spatial resolution. Second, in order to provide an anatomical template for visualizing the group statistical maps, individual anatomical images were transformed to 1×1×1 mm MNI-152 space and then were averaged across participants.

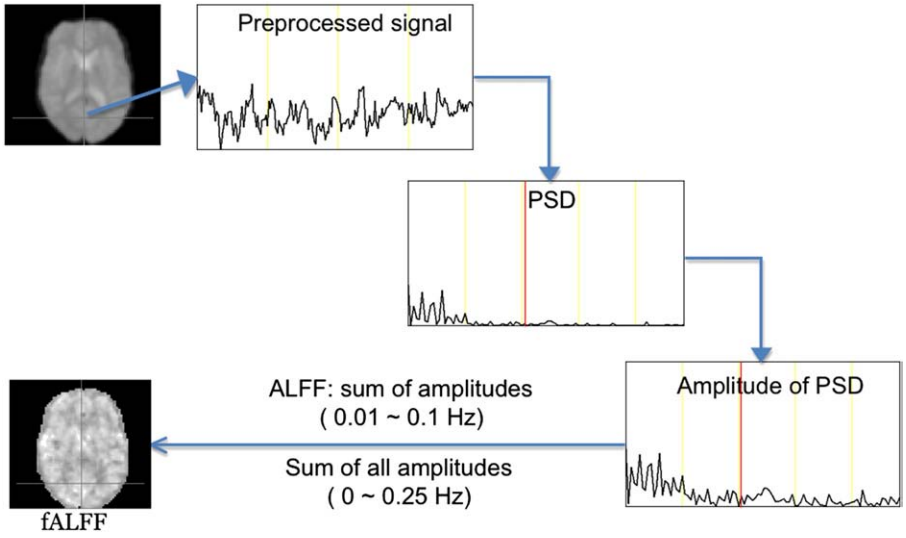


**Fig. 1.** Computational diagram for individual amplitude of low frequency fluctuations (ALFF) and fractional ALFF (fALFF) maps. This sketch summarizes the main steps taken to conduct power spectral density (PSD) analyses of the resting state fMRI signal and to compute the amplitude measures of low frequency oscillations implemented here: the amplitude of low frequency fluctuations (ALFF), and the fractional ALFF (fALFF). All calculations are done in a participant's native space. The red line is at 0.1 Hz. For group-level statistical analysis, these ALFF and fALFF maps are converted into *Z*-score maps by subtracting mean and dividing standard deviation within a whole brain mask for the participant.

*Group voxel-wise analyses*

Group-level analyses were carried out using a mixed-effects model (as implemented in the FSL program FLAME). First, a fixed-effects analysis was carried out for each participant, which combined all three scans for each participant. We then performed a standard mixed-effect analysis on these fixed-effects results. Cluster-based statistical corrections for multiple comparisons were performed using Gaussian random field theory ($Z>2.3$; $p<0.05$, corrected). This group-level analysis produced thresholded $Z$-statistic maps showing brain regions with significantly detectable ALFF or fALFF (i.e., differing significantly from the global brain baseline of ALFF or fALFF). The group-level ALFF map shows those brain areas that exhibited LFO amplitudes that were significantly higher than the baseline, across subjects. The group-level fALFF map shows those regions whose contribution to the low frequency amplitudes was significantly higher than the baseline.

As suggested in the original fALFF paper (Zou et al., 2008), because fALFF provides a ratio of power at low frequencies to the power of lower and higher frequencies within the range sampled by a given fMRI BOLD signal, fALFF may provide a more reasonable measure of LFO that controls for contributions from several nuisance sources. Such nuisance signals are likely to have a different spatial distribution to that of neurophysiologically meaningful LFO. We therefore tested for differences between ALFF and fALFF by performing a paired-test on the individual fixed-effects maps. Multiple comparisons correction based on Gaussian random field theory ($Z>2.3$; $p<0.05$, cluster-level corrected) was applied. This group-level analysis generated $Z$-statistic maps of regions in which ALFF differed significantly from fALFF. We used a peak detection algorithm as implemented in the AFNI command (*3dmaxima*) to identify peaks for the group-level $Z$-statistic maps using a minimum threshold of $Z \geq 2.3$ and minimum distance between peaks of 20, 2-mm isomorphic voxels.

In order to demonstrate previously reported distinctions between gray and white matter with respect to LFO amplitudes, voxels were labeled as gray, white and neither, based upon corresponding 152-brain average tissue prior maps (MNI152 space) provided by FSL (tissue belong probability threshold = 50%).

*Test–retest reliability analyses*

To investigate the test–retest reliability of ALFF and fALFF, we calculated intraclass correlation (ICC), a common index of test–retest reliability (Shrout and Fleiss, 1979). For each brain unit (e.g., voxel), the ALFF (or fALFF) was first merged into two $26\times2$ ALFF (or fALFF) matrices. Here the two $26\times2$ matrices can represent ALFF (or fALFF) across scans 2 and 3 (intra-session, short-term reliability) or between scan 1 and the average of scans 2 and 3 (inter-session, long-term reliability). Scans 2 and 3 were averaged to improve the estimation of long-term reliability. Using a one-way ANOVA on each of the two matrices, with random subject effects, we split the total sum of the squares into between-subject ($MS_b$) and within-subject ($MS_w$, i.e., residual error) sum of squares. ICC values were subsequently calculated according to the following equation where $k$ is the number of repeated observations per subject (Shrout and Fleiss, 1979):

$$ICC = \frac{MS_b - MS_w}{MS_b + (k-1)MS_w}. \quad (3)$$

As per equation (3), for a measure to be reliable (exhibiting high ICC) there should be low within-subject variance relative to between-subject variance. Thus, ICC ranges from 0 (no reliability) to 1 (perfect reliability) and can be understood as a measure of discrimination between participants (Bland and Altman, 1996). We used the same methods of peak detection applied to the group-level $Z$-statistic maps to detect ICC peaks (thresholded at ICC ≥ 0.5).

*Region-based analysis*

Parcellation-based masks were generated from the 50% probability thresholded Harvard-Oxford Structural Atlas, a probabilistic atlas that defines regions based on standard anatomical boundaries (Kennedy et al., 1998; Makris et al., 1999). Masks overlapping the midline were divided at $X=0$, creating a total of 110 regional masks (55 in each hemisphere). ALFF and fALFF measures were calculated for each parcellation region from the mean $Z$-score in the region. For each participant, ALFF and fALFF measures were obtained for each scan separately and then averaged. The Friedman test was used to examine the presence of a significant ordering of anatomical regions with respect to each of the amplitude measures (ALFF and fALFF).

*Decomposing LFO in different frequency bands*

We subdivided the low frequency range into four bands as previously defined (Buzsáki and Draguhn, 2004; Penttonen, 2003): slow-5 (0.01–0.027 Hz), slow-4 (0.027–0.073 Hz), slow-3 (0.073–0.198 Hz) and slow-2 (0.198–0.25 Hz). We computed group level ALFF and fALFF spatial maps and ICC for all four bands (slow-5, slow-4, slow-3 and slow-2) in the same manner as for the primary broadband analysis. To further examine region-based differences in LFO amplitude between these slow bands, for each of four slow bands, we computed the percentage of voxels exhibiting significantly detectable ALFF (or fALFF) for each of the 110 Harvard–Oxford parcellation units.

Of note, the frequencies subtended by the slow-5 and slow-4 bands are those typically utilized for RSFC analyses (0.01–0.1 Hz). To test for the presence of regional differences in significantly detectable LFO amplitude at the two bands, we carried out paired tests using a mixed-effect group analysis between the slow-5 and slow-4 bands for each of the measures (ALFF and fALFF).

## Results

*Analytic overview*

We divided our examination of LFO into three domains of investigation. First, based on resting state fMRI timeseries' power spectral density, we systematically characterized the spatial distributions of both LFO amplitude measures (ALFF and fALFF) (Zou et al., 2008) within the traditional low frequency range (0.01–0.1 Hz). Second, we evaluated short-term or intra-session (<1 h) test–retest reliability and long-term or inter-session (>5 months) test–retest reliability for each of the two amplitude measures. Finally, we provided a more comprehensive examination of the power spectrum of the spontaneous BOLD fluctuations by subdividing it into four different slow frequency ranges based on prior work (slow-5: 0.01–0.027 Hz, slow-4: 0.027–0.073 Hz, slow-3: 0.073–0.198 Hz, slow-2: 0.198–0.25 Hz) (Buzsáki and Draguhn, 2004; Di Martino et al., 2008a; Penttonen, 2003). For each of these subdivisions, we repeated our primary analyses and compared the spatial distribution and test–retest reliability of the signals observed.

*Amplitude measures of oscillatory fMRI waves*

As previously reported (Biswal et al., 1995, 1997; Cordes et al., 2001; Jezzard et al., 1993; Yan et al., 2009), LFO amplitudes were consistently greater in gray matter than in white matter. Specifically, across participants, paired $t$-tests (one for each scan) showed that mean ALFF observed for voxels located within gray matter was consistently greater than mean ALFF for voxels within white matter (scan 1: $p<1\times10^{-21}$; scan 2: $p<1\times10^{-22}$; scan 3: $p<1\times10^{-22}$; see Fig. 1C and Figure S1). Similarly, mean fALFF for voxels within gray matter was consistently greater across participants than measures obtained within

white matter (scan 1: $p<1\times10^{-12}$; scan 2: $p<1\times10^{-11}$; scan 3: $p<1\times10^{-11}$; see Fig. 2C and Figure S1). Together, these findings reaffirm earlier results that LFO amplitudes are markedly greater in gray matter than white matter.

ALFF and fALFF exhibit highly similar distributions among gray matter regions, particularly within the cortex (see Fig. 2A and B). Areas of maximal significance for both ALFF and fALFF measures included visual cortex, posterior cingulate cortex/precuneus, thalamus, medial prefrontal cortex, anterior cingulate cortex, temporal gyrus and lateral frontal cortex (see Table S1 for complete listing of peak activations). As indicated by Kendall's coefficient of concordance (Legendre, 2005), the group statistical maps for the two measures (ALFF and fALFF) are highly similar, but not entirely concordant ($W=0.9005$).

Accordingly, in order to identify areas of difference between the two measures, we compared *Z*-scores for ALFF and fALFF at each voxel using paired *t*-tests across participants. Consistent with a prior report by Zou et al. (2008), ALFF was markedly greater than fALFF near large blood vessels, and in areas adjacent to CSF (particularly in the brainstem), which are susceptible to the effects of pulsatile motion (Fig. 3A $Z>2.3$, $p<0.05$, cluster-level corrected). These differences between ALFF and fALFF suggest that in perivascular and periventricular areas, LFO are more likely to reflect vascular pulsatility (e.g., aliasing of cardiac signal, Meyer waves) rather than neuronal fluctuations (Dagli et al., 1999; Julien, 2006).

In further characterizing voxels exhibiting significantly greater ALFF than fALFF, we noted that 76.5% were located within gray matter, 3.4% in white matter and 20.1% in neither compartment (i.e., blood vessels and CSF). The gray matter voxels exhibiting significantly greater ALFF than fALFF accounted for 15.3% of total brain gray matter. Of note, among voxels exhibiting greater ALFF compared to fALFF, those within gray matter still exhibited higher fALFF levels than the voxels not located in gray matter (Fig. 3C). Thus, despite increased noise in perivascular and periventricular regions, gray matter is characterized by greater LFO amplitude, relative to white matter.

Beyond gross distinctions in LFO amplitude measures among gray and white matter, we also tested for amplitude differences among anatomical regions. We did so by rank-ordering brain regions based upon ALFF and fALFF. Specifically, we divided the brain into 110 anatomical units (55 in each hemisphere) based on the Harvard-Oxford Atlas (50% threshold criteria were employed, see Table 1 for a list of all parcellation units and their abbreviations) (Kennedy et al., 1998; Makris et al., 1999). For each participant, ALFF and fALFF measures were calculated for each region by averaging ALFF and fALFF *Z*-scores within the region. Since each participant had three scans, ALFF and fALFF measures were obtained for each scan separately, and then averaged across scans. For both ALFF and fALFF, we tested for the presence of a significant ordering of anatomical regions with respect to the corresponding amplitude measure (the Friedman test denotes whether the within-subject rankings of a measure differ systematically between subjects). Significant orderings were observed for both measures (ALFF in left hemisphere: $\chi^2_{54}=100.72$, $p=1.0\times10^{-4}$; ALFF in right hemisphere: $\chi^2_{54}=122.33$, $p=3.25\times10^{-7}$; fALFF in left hemisphere: $\chi^2_{54}=104.82$, $p=4.18\times10^{-5}$; fALFF in right hemisphere: $\chi^2_{54}=110.47$, $p=9.29\times10^{-6}$) with visual and posteromedial cortices (precuneus, posterior cingulate) being among the highest ranked for both measures (see Fig. 4 and Figure S2). Of note, some regions differed markedly in their relative rankings for ALFF and fALFF. Consistent with our voxel-based analyses, portions of the temporal lobe and subcortical regions (e.g., pallidum and brainstem,

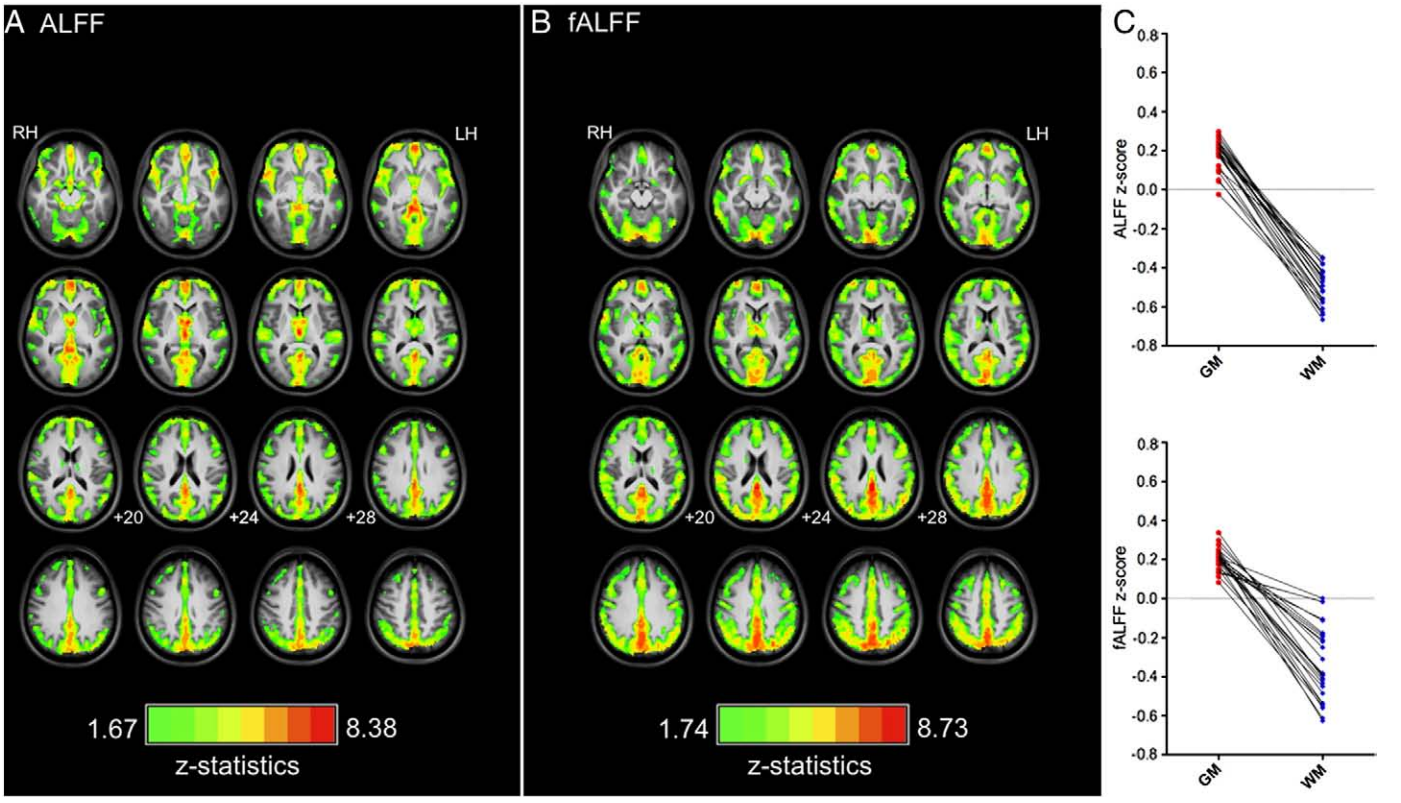


**Fig. 2.** Amplitude of spontaneous low frequency oscillations in the resting brain. (A) Group-level *Z*-statistic maps showing significantly detectable amplitude of low frequency fluctuations (ALFF) across the whole brain. A one-sample statistical test was carried out combining a fixed-effects model (within participant) with a mixed-effects model (across participants: see Methods for details). Cluster-level multiple comparisons correction was performed using Gaussian random field theory ($Z>2.3$; $p<0.05$, corrected). (B) Group-level *Z*-statistic maps showing significantly detectable fractional ALFF (fALFF) across the whole brain. The statistical test is the same as in (A). (C) Mean voxel-wise ALFF and mean voxel-wise fALFF were greater for gray matter (GM) than white matter (WM) across participants. LH = left hemisphere; RH = right hemisphere.

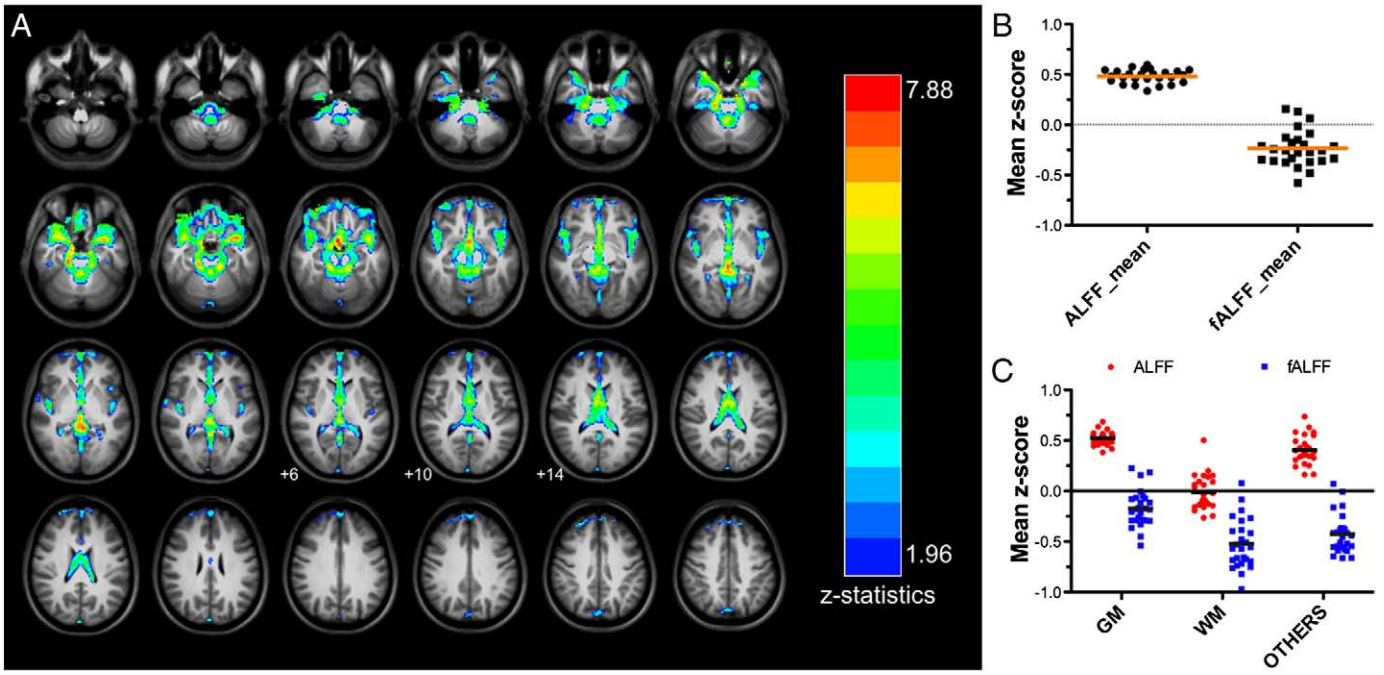


**Fig. 3.** Brain areas with higher amplitude of low frequency fluctuations (ALFF) than fractional ALFF (fALFF). (A) Group-level *Z*-statistic maps showing regions with significantly higher standardized ALFF than fALFF. Using standardized ALFF and fALFF (i.e., *Z*-scores), a paired two-sample statistical test was carried out (see Methods). Cluster-level multiple comparisons correction was performed using Gaussian random field theory ($Z>2.3$; $p<0.05$, corrected). (B) The scatter plot shows averaged ALFF and fALFF *Z*-score for all voxels within a mask selected to comprise the regions exhibiting higher ALFF than fALFF *Z*-scores in (A). (C) The scatter plot shows the mean ALFF and fALFF *Z*-score within gray matter (GM), white matter (WM) and other (CSF, vasculature) constrained with the mask depicted in (B). The generation of these three ROIs within the mask depicted in B (GM, WM and other) is detailed in the Methods section. LH = left hemisphere; RH = right hemisphere.

see Table 1) most likely to be affected by vascular and pulsatile effects exhibited marked differences between their ALFF and fALFF rankings (i.e., ALFF >> fALFF).

*Test–retest reliability of amplitude measures on oscillatory fMRI waves*

In order to assess the test–retest reliability of LFO amplitude measures, we calculated the voxel-wise intra- and inter-session ICC for both ALFF and fALFF (Fig. 5A). Voxels within gray matter generally exhibited moderate to high test–retest reliability, while those within white matter were characterized by low test–retest reliability (see Fig. 5B). For both ALFF and fALFF, areas of maximal ICC (intra- and inter-session) were located within anterior cingulate cortex, posterior cingulate cortex, medial prefrontal cortex, thalamus, inferior parietal lobule, superior temporal gyrus, inferior frontal gyrus, middle frontal gyrus and superior frontal gyrus (see Table S2 for a detailed maximal ICC listing).

While both measures (ALFF and fALFF) exhibited moderate to high test–retest reliability within gray matter regions, reliability for ALFF tended to be higher than for fALFF. At least in part, this difference can be explained by the fact that fALFF is a proportional measure (Arndt et al., 1991). This finding suggests that ALFF is more reliable than fALFF in gray matter regions, and thus potentially more sensitive for discerning differences between individuals and groups.

Finally, we examined whether or not regional differences in LFO amplitude measures (ALFF and fALFF) are consistent across intra- and inter-session scans. In order to accomplish this, we examined the Pearson correlation of LFO amplitude rank orderings for all parcellation units between the intra- and inter-session scans. Within and between sessions, we found highly consistent rank orderings of ALFF and fALFF for the 110 brain regions examined both at the group level (Fig. 6A) and at the individual level (Fig. 6B). Supplementary results provide further verification of the consistency of these regional findings, as they were reliable across two different scanner sites with distinct sets of participants (see Supplementary Text "Verification of Ranking Orders of Parcellation-Based LFO Amplitudes"). Further, supplementary analyses suggest that vascular effects alone do not appear to produce these regional differences, highlighting potential neural contributions (see Figure S3).

*Oscillatory fMRI waves in different frequency bands*

Penttonen and Buzsáki observed that neuronal oscillations are distributed linearly on the natural logarithmic scale (Buzsáki and Draguhn, 2004; Penttonen, 2003). We applied Buzsáki's nomenclature by implementing an approach previously used to subdivide the frequency spectrum (Di Martino et al., 2008a). Accordingly, we reanalyzed our data using the following divisions: slow-5 (0.01–0.027 Hz), slow-4 (0.027–0.073 Hz), slow-3 (0.073–0.198 Hz) and slow-2 (0.198–0.25 Hz; note: the upper bound was constrained by the repetition time of the BOLD acquisition). Voxel-wise ALFF and fALFF maps for each of the four low-frequency bands are presented in Figure S4. For both ALFF and fALFF measures, significant slow-4 and slow-5 oscillations were primarily detected within gray matter. In contrast, slow-3 and slow-2 oscillations were primarily restricted to white matter (Fig. 7 and S4). This distinction of slows 2/3 vs. slows 4/5 is especially noteworthy given prior demonstrations that respiratory and aliased cardiac signals fall in the range of slows 2–3 (Cordes et al., 2001), while the oscillatory signals upon which resting state functional connectivity is based are primarily located within slows 4–5 (De Luca et al., 2006; Salvador et al., 2008). In order to summarize differences in the distribution of fALFF among each of the four frequency bands as well as the classic (<0.1 Hz) low frequency band, we computed and visualized the percentage of significantly detectable voxels within each of the 110 anatomical parcellation units previously described (Figure S5). This analysis was limited to fALFF since ALFF is more likely to include artifacts that disproportionately impact subcortical and periventricular regions.

Focusing on slows 4 and 5, which were both broadly distributed through gray matter, voxel-wise paired comparisons of slow-4 and

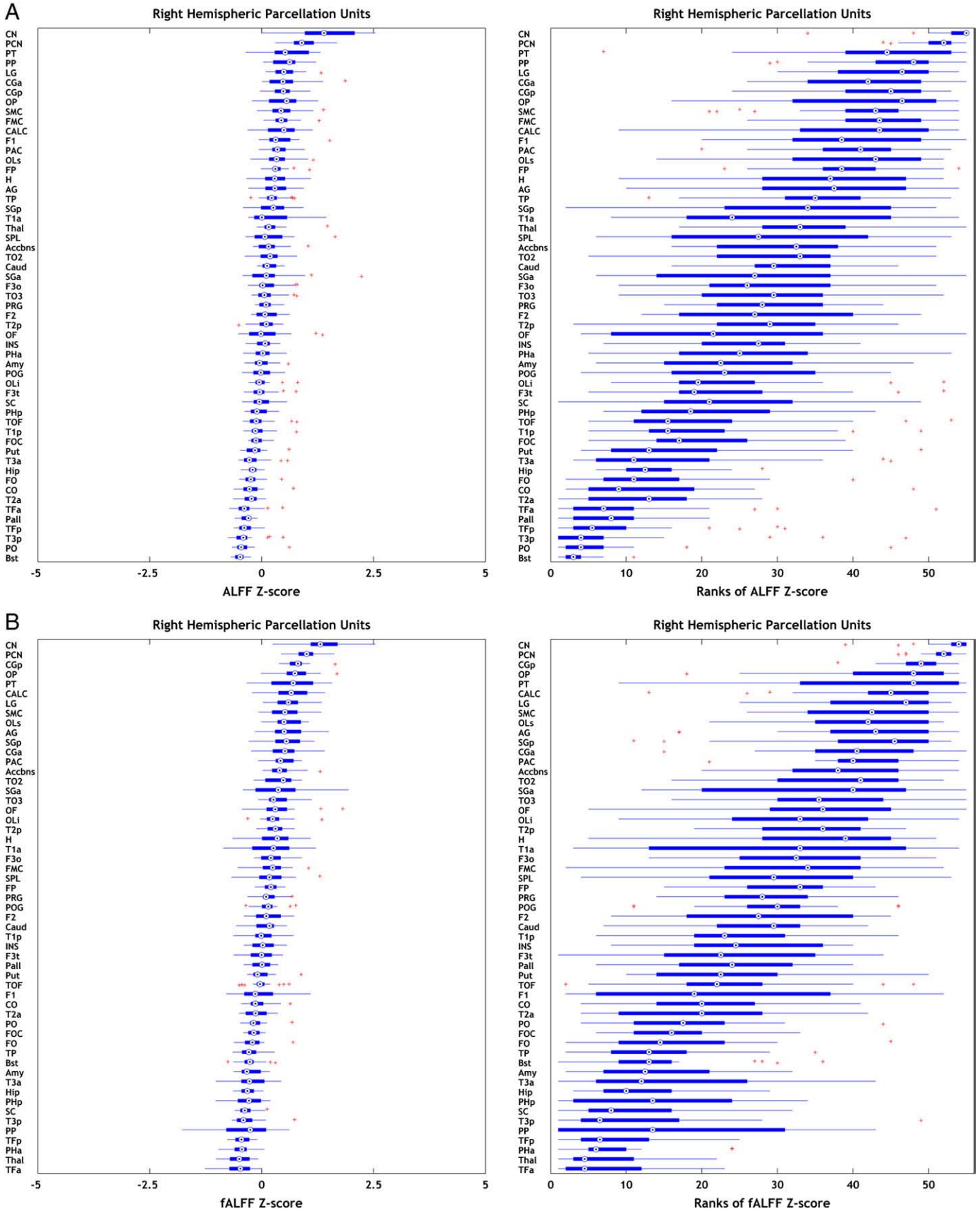


**Fig. 4.** Parcellation-based amplitude of low frequency fluctuations (ALFF) and fractional ALFF (fALFF) and their ranking orders. The figure depicts Tukey box-and-whiskers plots showing the distribution of (A) right hemispheric ALFF *Z*-scores and ranked ALFF *Z*-scores and of (B) right hemispheric fALFF *Z*-scores and ranked fALFF *Z*-scores for all 55 parcellation regions across participants (circle with center black point = median; blue box = interquartile range; blue whiskers = 1.5 times the interquartile range; red crosses = individual values lying outside 1.5 times the interquartile range). All abbreviations for parcellation region names are listed in Table 1.

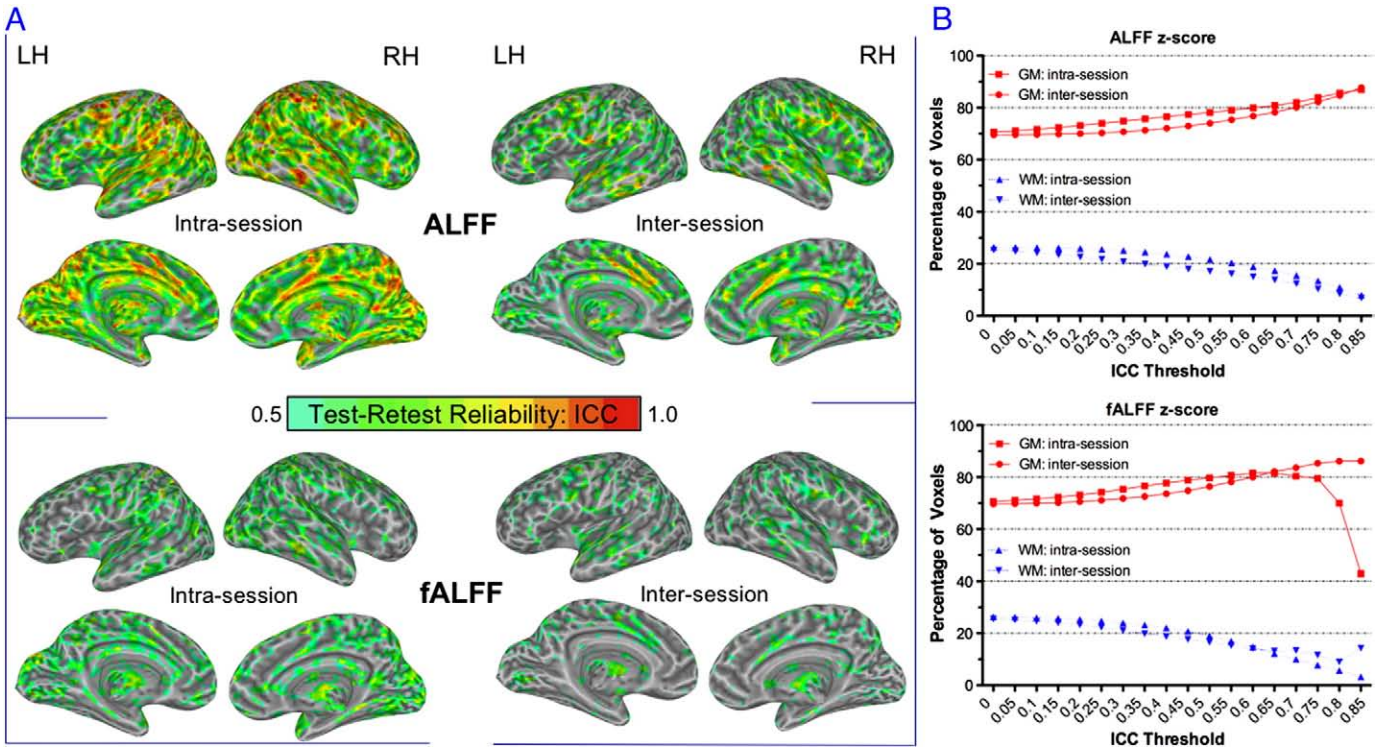


**Fig. 5.** Test–retest reliability maps on standardized amplitude of low frequency fluctuations (ALFF) and fractional ALFF (fALFF). (A) This figure depicts the voxel-wise ICC maps showing the intra- and inter-session (left and right column, respectively) test–retest reliability for each of the two LFO amplitude measures examined in this study: ALFF and fALFF (top and bottom row, respectively). Only the regions with high reliability (ICC > 0.5) are shown. As evident by inspection of these ICC maps ALFF has greater reliability than fALFF. (B) The graphs indicate the percentage of gray matter (GM) and white matter (WM) voxels above each ICC threshold ranging from 0 to 0.85 for ALFF and fALFF (top and bottom graph, respectively). LH = left hemisphere; RH = right hemisphere.

slow-5 revealed some noteworthy differences. Compared to slow-5, slow-4 fALFF was higher throughout the basal ganglia, thalamus and several sensorimotor regions and was lower within ventromedial regions (Fig. 8).

Finally, we examined the test–retest reliability of slow-5 and slow-4. Specifically, we calculated the voxel-wise intra- and inter-session ICC for both ALFF and fALFF in these two slow bands. Figure S6 presents the sphere maps of test–retest reliability showing voxels with significantly detectable LFO amplitudes and high test–retest reliability (i.e., ICC $\geq$ 0.5). On visual inspection, slow-4 demonstrates greater and more widely distributed intra-session ICC values than slow-5. Moreover, to provide a more comprehensive examination of the spatial distribution of ICC values for both slow bands, we used distinct ICC thresholds for slow-5 and slow-4 and then computed the percentage of reliable voxels within gray matter. The results indicate that for both ALFF and fALFF, slow-4 has higher test–retest reliability and more widespread spatial distribution of reliable voxels than slow-5 (see Figure S7).

We considered the possibility that our differential findings for the four slow bands may have reflected differences in the number of samples in the power spectrum for each of the frequency bands, rather than their specific spectral properties. Accordingly, we reanalyzed our data using the same number of samples in each band (centered around each band's middle frequency). A highly consistent pattern of findings was obtained, mitigating concern about this possible confound.

## Discussion

Several observations emerged from this examination of spontaneous LFO in the human brain at rest. Beyond confirming prior demonstrations of higher LFO amplitude within gray matter (Biswal et al., 1995; Cordes et al., 2001), we found that ALFF measures in the brain are more susceptible to gross pulsatile effects, and that these are attenuated in fALFF. Despite these differences in sensitivity to artifacts, both ALFF and fALFF exhibit regional differences within the brain, with the largest amplitudes found along the midline and in visual cortices. We also found that both ALFF and fALFF exhibit moderate to high intra- and inter-session test–retest reliability throughout the brain, though primarily in gray matter. Furthermore, we found that rankings of regional differences in LFO amplitude measures are strikingly consistent, showing little variability within or across sessions. Supplementary analyses conducted on an independent dataset suggest that these regional differences generalize to other scanners and are not simply attributable to vascular effects. Finally, our analyses of four previously characterized subdivisions of the power spectrum suggest that (1) gray matter related oscillations primarily occur in the slow-4 and slow-5 range (0.01–0.073 Hz), (2) slow-4 fluctuations are more robust in basal ganglia than slow-5, while slow-5 is more dominant within ventromedial prefrontal cortices than slow-4, and (3) although robust for both, test–retest reliability was greater and more widely distributed for slow-4 than for slow-5.

In considering the areas exhibiting maximal LFO amplitudes, we note that many are components of what has come to be known as the "default-mode" network. Characterized by greater metabolic and neural activity during rest than active task performance, activity within this medial wall-based network has been proposed to reflect a physiological baseline for the brain (Gusnard and Raichle, 2001; Raichle, 2009; Raichle et al., 2001; Raichle and Mintun, 2006). Our finding of greater reliability in these medial wall structures is consistent with the conclusion that these regions represent the functional core underlying resting brain dynamics, a notion recently supported by a computational model of the resting brain and network analyses combining functional and structural measures (Ghosh et al., 2008; Hagmann et al., 2008; Honey et al., 2009). These same regions

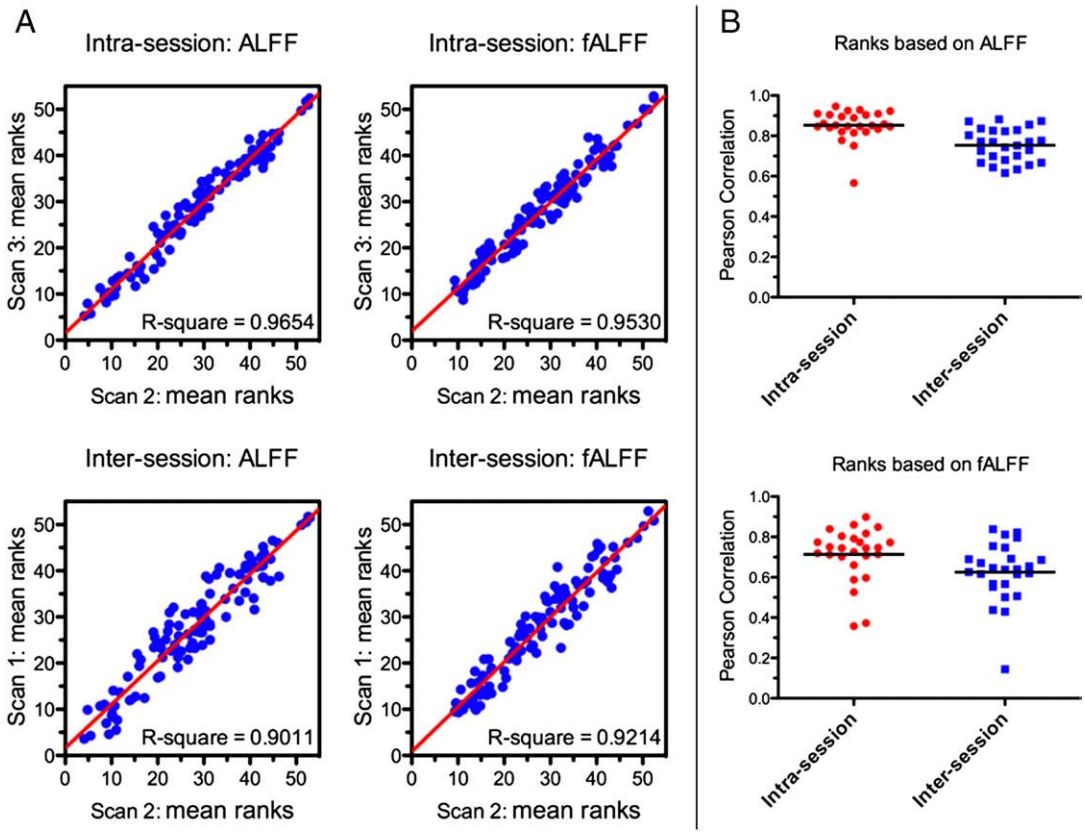


**Fig. 6.** Reliable rank ordering for anatomical parcellation. Given that each participant had three scans, standardized amplitude of low frequency fluctuations (ALFF) and fractional ALFF (fALFF) measures (i.e., *Z*-scores) were obtained for each parcellation region separately for each scan. The parcellation regions were then ranked based upon their standardized ALFF and fALFF. For each scan, the mean rank for a parcellation region was obtained by averaging all individual ranks for the region. (A) The reliability of mean ranks. (B) The reliability of subject-level ranks. Overall these panels illustrate the consistency of ALFF- and fALFF-based rank orderings for the parcellation regions over the short- and long-term (intra-session and inter-session, respectively).

show marked reductions in LFO amplitudes during task performance, suggesting a discernible redistribution of resources associated with attentional and cognitive demands (Duff et al., 2008; Fransson, 2006). Ongoing work will examine the impact of attentional states and cognitive demands on LFO.

### *Origins and potential significance of spontaneous low-frequency fluctuations*

Despite the increasing popularity of studies of spontaneous fluctuations in the BOLD signal, the origins and functional significance of LFO remain unclear (Bianciardi et al., 2009; Buckner and Vincent, 2007). The spectral coincidence between BOLD signal LFO and fluctuations of systemic vascular phenomena (Shmueli et al., 2007), such as Mayer waves (Julien, 2006), has led to the suggestion that BOLD LFO reflect cardiovascular or respiratory fluctuations (Birn et al., 2006; Birn et al., 2008; Chang et al., 2009; Shmueli et al., 2007; van Buuren et al., 2009). However, a recent application of near-infrared optical topography approaches capable of distinguishing cerebral pulsations from cardiovascular phenomena suggests that cerebral LFO are at least partially independent of cardiovascular fluctuations (Yamazaki et al., 2007). Some authors have suggested that spontaneous low-frequency fluctuations in the BOLD signal may be the byproduct of low-pass filtering via neurovascular coupling, rather than reflecting low-frequency fluctuations present in neural activity. However, a recent study of visual stimulation found that such filtering is insufficient to explain BOLD LFO phenomena (Anderson, 2008).

In considering the major candidates capable of producing low-frequency phenomena, increasing evidence is mounting for neural activity as the primary contributor (Balduzzi et al., 2008). First, the dominance of LFO in gray matter compared to white matter, together with studies of fMRI dynamics showing greater persistence or long-memory in gray matter regions (Suckling et al., 2008; Wink et al., 2008), suggest a possible link to neuronal processes. Our findings of greater test–retest reliability for LFO amplitudes in gray matter provide further support for such a link. Moreover, our supplementary analyses, showing preservation of regional rank ordering of ALFF and fALFF measures during breath-holding, a condition that markedly disrupts vascular dynamics, further support the contributions of neural processes.

Potentially the most intriguing are recent studies directly linking BOLD oscillations to those observed in EEG. For example, by recording full-bands and resting-state BOLD signals simultaneously, He et al. (2008) directly related BOLD LFO to infra-slow fluctuations (<0.1 Hz) observed in neuronal activity. Although long considered as noise in the EEG literature, meaningful infra-slow fluctuations are increasingly being appreciated in EEG studies of humans (Monto et al., 2008), as well as monkeys (Leopold et al., 2003) and rats (Chen et al., 2009). Similarly, recent work has demonstrated low-frequency amplitude modulation of various higher frequency signals (i.e., delta, alpha, beta, gamma) (Lu et al., 2007; Mantini et al., 2007).

In considering the potential significance of low-frequency neural fluctuations, several authors have drawn attention to variations in cortical excitability and in cognitive performance (Fox et al., 2007; Monto et al., 2008). Fox et al. (2007) found a significant relationship between resting state brain activity and the spontaneous trial-to-trial variability of button press force in somatomotor cortex. More recently, the phase of EEG LFO has been linked to the slow fluctuations in human psychophysical performance during a somatosensory detection task (Monto et al., 2008). In a behavioral study, the response time

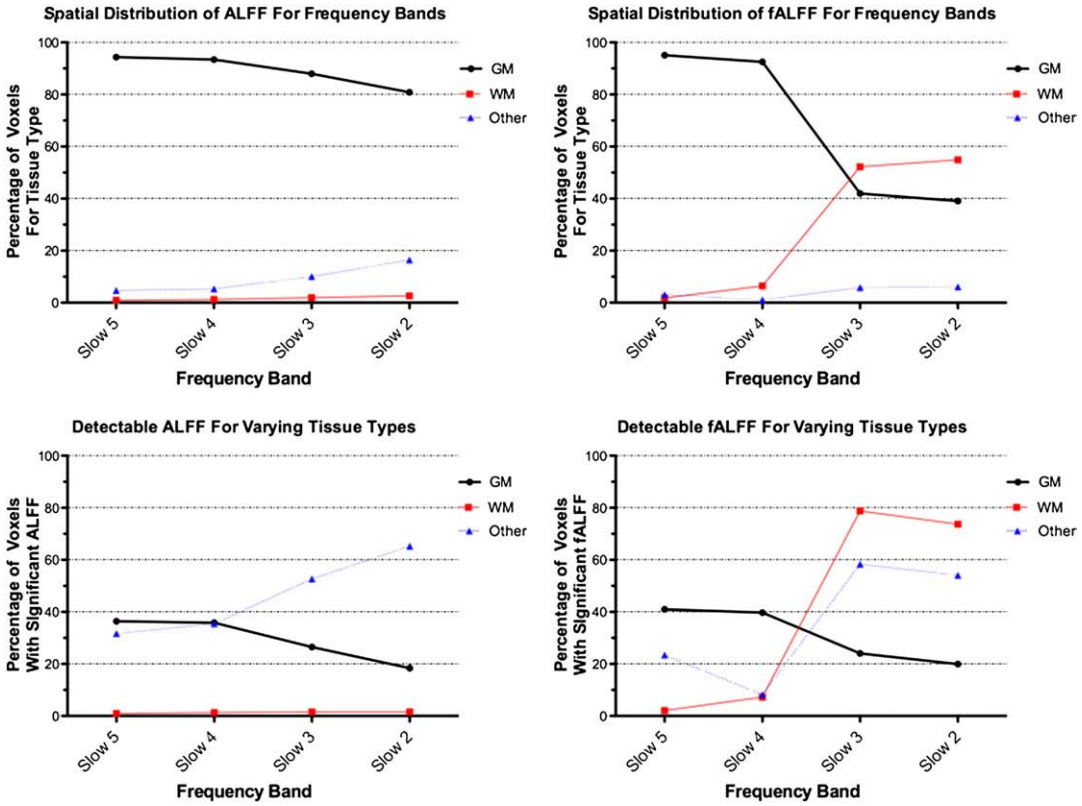


**Fig. 7.** Tissue distribution of amplitude of low frequency fluctuations (ALFF) and fractional ALFF (fALFF) for different frequency bands. For each amplitude measures (i.e., ALFF and fALFF), the percentage of voxels within a tissue-type: gray matter (GM), white matter (WM), and others and the percentage of voxel with the significant amplitude measure were calculated for four frequency bands defined as follows: Slow-5 (0.01–0.027 Hz), Slow-4 (0.027–0.073 Hz), Slow-3 (0.073–0.198 Hz), Slow-2 (0.198–0.25 Hz).

fluctuations of children with ADHD exhibited significantly greater power within the slow-4 range (Di Martino et al., 2008a). We note that we found slow-4 LFO to be particularly prominent in the basal ganglia — a key putative site of dysfunction in ADHD (Bush et al., 2005; Castellanos and Tannock, 2002). Intriguingly, similar oscillations (~0.028 Hz) evident in basal ganglia neuronal recordings from awake, locally anesthetized rats, are selectively modulated by low doses of dopaminergic drugs such as those used to treat ADHD (Ruskin et al., 1999a,b, 2001). Thus, our findings add to the increasing body of evidence that slow-4 neuronal fluctuations characterize basal ganglia spontaneous intrinsic activity (Hutchison et al., 2004).

*Test–retest reliability of LFO amplitude measures*

While prior work has suggested that LFO amplitudes may be affected by a variety of factors (Biswal et al., 1997; Fransson, 2006; Kiviniemi et al., 2000, 2005; McAvoy et al., 2008; Suckling et al., 2008; Yang et al., 2007), our findings suggest that inter-individual differences in LFO amplitudes are relatively stable. Both ALFF and fALFF exhibited encouraging test–retest reliabilities. First, the LFO amplitude measures derived from gray matter were markedly more reliable than those derived from white matter. That gray matter exhibits higher-amplitude LFO and higher test–retest reliability, relative to white matter, is consistent with the idea that BOLD LFO reflects meaningful neuronal activity, which is absent from white matter. Second, the parcellation-based reliability analyses demonstrated a highly consistent and reliable rank ordering of LFO amplitudes across the brain. The robustness of these findings, both across subjects and scanners, indicate a potential area of interest for future studies of the functional architecture in brain, as well as the possible impact of developmental and pathological processes (Greicius et al., 2009; Honey et al., 2009; van den Heuvel et al., 2009).

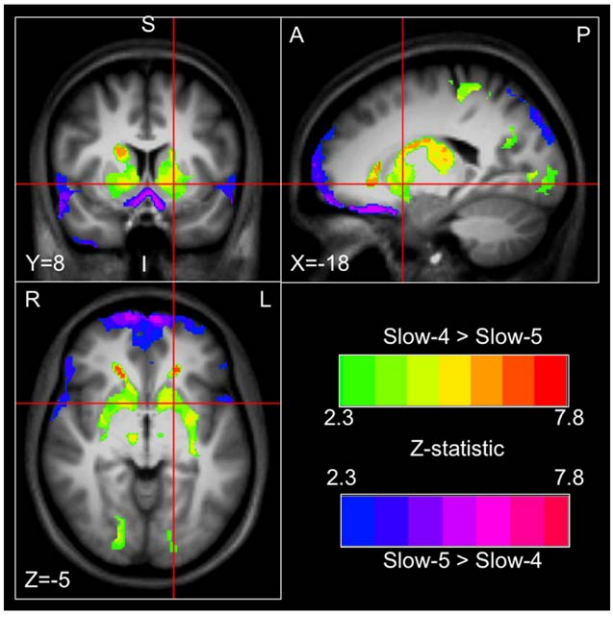


**Fig. 8.** Spatial regions with higher fractional amplitude of low frequency fluctuations (fALFF): Slow-4 versus Slow-5. Color maps depict voxels exhibiting significant differences in fALFF obtained for the slow-4 and slow-5 bands, as detected by paired two-sample statistical test carried out using a mixed-effect. Cluster-level multiple comparisons correction was performed using Gaussian random field theory ($Z>2.3$; $p<0.05$, corrected). As illustrated, compared to Slow-5, Slow-4 fALFF measures were significantly greater in the basal ganglia and significantly lower in the medial prefrontal cortex.

**Table 1**
Mean ALFF and fALFF *Z*-scores and ranking across scans and participants for parcellation regions.

| Parcellation regions | | ALFF: RH | | ALFF: LH | | fALFF: RH | | fALFF: LH | |
|---|---|---|---|---|---|---|---|---|---|
| Full name | Abbreviation | *Z* | R | *Z* | R | *Z* | R | *Z* | R |
| Cuneal cortex | CN | 1.450 | 55 | 1.465 | 55 | 1.381 | 55 | 1.377 | 55 |
| Precuneus cortex | PCN | 0.929 | 54 | 1.093 | 54 | 1.013 | 54 | 1.152 | 54 |
| Planum temporale | PT | 0.601 | 53 | 0.332 | 43 | 0.705 | 51 | 0.296 | 35 |
| Planum polare | PP | 0.590 | 52 | 0.494 | 50 | −0.344 | 5 | −0.448 | 3 |
| Lingual gyrus | LG | 0.531 | 51 | 0.627 | 53 | 0.595 | 49 | 0.644 | 51 |
| Cingulate gyrus, anterior division | CGa | 0.508 | 50 | 0.518 | 51 | 0.528 | 44 | 0.539 | 46 |
| Cingulate gyrus, posterior division | CGp | 0.495 | 49 | 0.548 | 52 | 0.790 | 53 | 0.840 | 53 |
| Occipital pole | OP | 0.495 | 48 | 0.315 | 42 | 0.744 | 52 | 0.559 | 48 |
| Supplementary motox cortex | SMC | 0.477 | 47 | 0.427 | 47 | 0.574 | 48 | 0.545 | 47 |
| Frontal medial cortex | FMC | 0.467 | 46 | 0.478 | 49 | 0.214 | 32 | 0.334 | 41 |
| Intracalcarine cortex | CALC | 0.453 | 45 | 0.458 | 48 | 0.695 | 50 | 0.695 | 52 |
| Superior frontal gyrus | F1 | 0.406 | 44 | 0.357 | 44 | −0.055 | 19 | 0.005 | 21 |
| Paracingulate gyrus | PAC | 0.398 | 43 | 0.374 | 45 | 0.473 | 43 | 0.475 | 45 |
| Lateral occipital cortex, superior division | OLs | 0.389 | 42 | 0.424 | 46 | 0.568 | 47 | 0.613 | 50 |
| Frontal pole | FP | 0.352 | 41 | 0.288 | 40 | 0.193 | 30 | 0.187 | 31 |
| Heschl's gyrus | H | 0.312 | 40 | 0.257 | 37 | 0.270 | 35 | 0.227 | 32 |
| Angular gyrus | AG | 0.305 | 39 | 0.293 | 41 | 0.564 | 46 | 0.604 | 49 |
| Temporal pole | TP | 0.262 | 38 | 0.104 | 33 | −0.245 | 13 | −0.371 | 8 |
| Supramarginal gyrus, posterior division | SGp | 0.243 | 37 | 0.093 | 30 | 0.546 | 45 | 0.416 | 43 |
| Superior temporal gyrus, anterior division | T1a | 0.235 | 36 | −0.076 | 16 | 0.244 | 34 | 0.018 | 23 |
| Thalamus | Thal | 0.229 | 35 | 0.186 | 36 | −0.509 | 2 | 0.154 | 30 |
| Superior parietal lobule | SPL | 0.181 | 34 | 0.286 | 39 | 0.196 | 31 | 0.298 | 36 |
| Accumbens | Accbns | 0.164 | 33 | 0.031 | 25 | 0.444 | 42 | 0.321 | 40 |
| Middle temporal gyrus, temporooccipital part | TO2 | 0.163 | 32 | 0.143 | 35 | 0.411 | 41 | 0.403 | 42 |
| Caudate | Caud | 0.160 | 31 | −0.184 | 12 | 0.101 | 26 | −0.093 | 18 |
| Supramarginal gyrus, anterior division | SGa | 0.158 | 30 | 0.098 | 31 | 0.396 | 40 | 0.422 | 44 |
| Inferior frontal gyrus, pars opercularis | F3o | 0.124 | 29 | 0.113 | 34 | 0.235 | 33 | 0.244 | 33 |
| Inferior temporal gyrus, temporooccipital part | TO3 | 0.121 | 28 | 0.102 | 32 | 0.374 | 39 | 0.304 | 38 |
| Precentral gyrus | PRG | 0.107 | 27 | 0.025 | 22 | 0.150 | 29 | 0.147 | 28 |
| Middle frontal gyrus | F2 | 0.102 | 26 | −0.055 | 17 | 0.133 | 27 | 0.060 | 25 |
| Middle temporal gyrus, posterior division | T2p | 0.082 | 25 | 0.026 | 23 | 0.276 | 36 | 0.259 | 34 |
| Occipital fusiform gyrus | OF | 0.050 | 24 | 0.062 | 28 | 0.347 | 38 | 0.319 | 39 |
| Insular cortex | INS | 0.047 | 23 | −0.020 | 19 | 0.037 | 24 | −0.050 | 20 |
| Parahippocampal gyrus, anterior division | PHa | 0.033 | 22 | −0.081 | 15 | −0.466 | 3 | −0.447 | 4 |
| Amygdala | Amy | 0.008 | 21 | −0.023 | 18 | −0.263 | 11 | −0.170 | 15 |
| Postcentral gyrus | POG | 0.004 | 20 | −0.011 | 20 | 0.134 | 28 | 0.154 | 29 |
| Lateral occiptal cortex, inferior division | OLi | −0.005 | 19 | 0.034 | 26 | 0.286 | 37 | 0.299 | 37 |
| Inferior frontal gyrus, pars triangularis | F3t | −0.005 | 18 | 0.048 | 27 | 0.013 | 23 | 0.099 | 26 |
| Subcallosal cortex | SC | −0.014 | 17 | 0.077 | 29 | −0.329 | 7 | −0.389 | 7 |
| Parahippocampal gyrus, posterior division | PHp | −0.068 | 16 | −0.097 | 14 | −0.305 | 8 | −0.309 | 11 |
| Temporal occipital fusiform cortex | TOF | −0.071 | 15 | −0.137 | 13 | −0.009 | 20 | 0.033 | 24 |
| Superior temporal gyrus, posterior division | T1p | −0.078 | 14 | −0.011 | 21 | 0.050 | 25 | 0.113 | 27 |
| Frontal orbital cortex | FOC | −0.098 | 13 | 0.031 | 24 | −0.166 | 15 | −0.141 | 17 |
| Putamen | Put | −0.147 | 12 | −0.343 | 8 | −0.008 | 21 | 0.011 | 22 |
| Inferior temporal gyrus, anterior division | T3a | −0.206 | 11 | −0.395 | 4 | −0.270 | 10 | −0.423 | 6 |
| Hippocampus | Hip | −0.209 | 10 | −0.194 | 11 | −0.303 | 9 | −0.273 | 12 |
| Frontal Opercular cortex | FO | −0.217 | 9 | −0.268 | 10 | −0.192 | 14 | −0.325 | 10 |
| Central opercular cortex | CO | −0.245 | 8 | −0.370 | 7 | −0.067 | 18 | −0.153 | 16 |
| Middle temporal gyrus, anterior division | T2a | −0.254 | 7 | −0.411 | 3 | −0.110 | 17 | −0.199 | 14 |
| Temporal fusiform cortex, anterior division | TFa | −0.336 | 6 | −0.370 | 6 | −0.519 | 1 | −0.557 | 1 |
| Pallidum | Pall | −0.336 | 5 | −0.495 | 1 | −0.001 | 22 | −0.233 | 13 |
| Temporal fusiform cortex, posterior division | TFp | −0.339 | 4 | −0.372 | 5 | −0.429 | 4 | −0.370 | 9 |
| Inferior temporal gyrus, posterior division | T3p | −0.385 | 3 | −0.455 | 2 | −0.338 | 6 | −0.446 | 5 |
| Parietal operculum cortex | PO | −0.406 | 2 | −0.326 | 9 | −0.142 | 16 | −0.055 | 19 |
| Brainstem | Bst | −0.496 | 1 | 0.260 | 38 | −0.253 | 12 | −0.503 | 2 |

LH = left hemisphere; RH = right hemisphere; *Z* = *Z*-score; R = ranking.

In recent years, a burgeoning literature has emerged examining the resting brain in clinical populations (Broyd et al., 2009; Greicius, 2008). With a few exceptions, amplitude measures have received relatively little attention. Instead, most studies have examined the impact of psychiatric and neurological illness on the spatial distribution of correlated low-frequency fluctuations, commonly referred to as functional connectivity. The present work suggests that analyses of LFO amplitudes may represent an additional potentially reliable and robust marker of inter-individual and group differences, with the advantage of being easily amenable to full-brain exploration. Fortunately, no new data collection is required to explore this possibility.

Despite the various forms of support for ALFF and fALFF measures provided by the present work, some noteworthy cautions emerge. Most notably, ALFF measures are more susceptible to possible artifactual findings in the vicinity of blood vessels and the cerebral ventricles, presumably reflecting pulsatile effects. The greater specificity of fALFF for gray matter appears to favor its use over that of ALFF. However, there is a cost, since ALFF has somewhat higher test–retest reliability in gray matter regions — not surprising given that fALFF is a ratio measure and thus intrinsically less reliable (Arndt et al., 1991). In the end, it is probably most advisable to report findings with both measures, taking into account their respective limitations, until a larger literature with these measures emerges to further guide selection.

*Limitations and future directions*

The present work has several potential limitations worth considering. Most notable is the lack of simultaneous measurement of cardiac and respiratory processes during the resting scan, as multiple studies using 3.0 and 7.0 T magnet strengths have drawn attention to the potential of physiological processes to contribute artifactual signals in the low-frequency range (Bianciardi et al., 2009; Birn et al., 2006; Chang et al., 2009; van Buuren et al., 2009; Yan et al., 2009). However, several points mitigate this concern. First, the impact of cardiac and respiratory-related processes on LFO phenomena within gray matter appears to be relatively small. Correction methods such as RETROICOR typically adjust the measures of LFO amplitudes by less than 5% in gray matter (Petridou et al., 2009). Second, our work demonstrated robust test–retest reliability throughout the entire brain, not simply regions that were previously reported to be influenced by respiratory or cardiac signals (Birn et al., 2006). Finally, our supplementary analyses show that the regional differences we demonstrated in ALFF were not markedly affected by breath-holding — a process that robustly manipulates the vascular contributions to the BOLD signal. In order to minimize artifactual contributions of respiratory and cardiac signals to LFO amplitude measures, our findings suggested that fALFF is generally more effective, particularly in perivascular, periventricular and periaqueductal regions (see Fig. 3).

Also worth noting is the choice to use the periodogram for power spectral density (PSD) to calculate LFO amplitudes and their reliability, consistent with prior work (Zang et al., 2007; Zou et al., 2008). Despite its ease of use and computation, the periodogram method is subject to sampling error or variability (Warner, 1998), which may negatively affect the estimation of test–retest reliability. Furthermore, it is insensitive to non-stationary characteristics of LFO appreciated by previous work (Bullmore et al., 2004; Maxim et al., 2005; Wink et al., 2008). In the future, it may be helpful to employ more robust methods of power spectra estimation (e.g., the Welch method, multi-tapers method or wavelet-based methods) (van Vugt et al., 2007). Another important factor for estimating the PSD is the repetition time (TR) used during fMRI scanning. In order to attain whole brain coverage, we used a TR = 2 s for our resting state fMRI scans. A faster TR can reduce frequency leakage and improve PSD resolution (Uitert, 1978), though at the cost of whole brain coverage and/or spatial resolution. Of note, previous studies comparing PSD results with slower (2 s) and faster TR's (e.g., 0.25–0.4 s) noted highly similar patterns of results in the low-frequency range, arguing in favor of slower repetition rates to increase spatial resolution and/or coverage (Biswal et al., 1995; De Luca et al., 2006; Yang et al., 2007).

## Concluding remarks

The current work represents the systematic and quantitative evaluation of the amplitude, spatial distribution and test–retest reliability of spontaneous LFO within the broad low-frequency range, and within four narrowly defined slow frequency bands. We observed differential spatial distribution of these LFO amplitudes within the resting brain, such that higher amplitude LFO were observed in gray matter, relative to white matter, and were particularly prominent along the midline of the brain. Detailed examination of individual low frequency bands showed distinct spatial profiles. In particular, LFO amplitudes in the slow-4 (0.027–0.073 Hz) band were most robust in the basal ganglia, as previously suggested by spontaneous electrophysiological recordings in the awake rat (Ruskin et al., 2001). Furthermore, we found that reliability ranged from minimal to robust. Our results provide a foundation for continued examination of LFO amplitude in typical and atypical populations. Our findings also shed further light on the potential neurophysiological significance of LFO.

## Acknowledgments

This work was partially supported by grants from NIMH (R01MH081218) and the Stavros S. Niarchos Foundation to F.X.C. and from the Leon Levy Foundation to M.P.M. and by gifts from Linda and Richard Schaps and Jill and Bob Smith to F.X.C. We wish to acknowledge the invaluable contributions of Dr. Yufeng Zang from Beijing Normal University and the two anonymous reviewers.

## Appendix A. Supplementary data

Supplementary data associated with this article can be found, in the online version, at doi:10.1016/j.neuroimage.2009.09.037.

## References

Anderson, J.S., 2008. Origin of synchronized low-frequency blood oxygen level-dependent fluctuations in the primary visual cortex. Am. J. Neuroradiol. 29, 1722–1729.
Arndt, S., Cohen, G., Alliger, R.J., Swayze II, V.W., Andreasen, N.C., 1991. Problems with ratio and proportion measures of imaged cerebral structures. Psychiatry Res. 40, 79–89.
Balduzzi, D., Riedner, B.A., Tononi, G., 2008. A BOLD window into brain waves. Proc. Natl. Acad. Sci. U. S. A. 105, 15641–15642.
Bianciardi, M., Fukunaga, M., van Gelderen, P., Horovitz, S.G., de Zwart, J.A., Shmueli, K., Duyn, J.H., 2009. Sources of functional magnetic resonance imaging signal fluctuations in the human brain at rest: a 7 T study. Magn. Reson. Imaging 27, 1019–1029.
Birn, R.M., Diamond, J.B., Smith, M.A., Bandettini, P.A., 2006. Separating respiratory-variation-related fluctuations from neuronal-activity-related fluctuations in fMRI. Neuroimage 31, 1536–1548.
Birn, R.M., Murphy, K., Bandettini, P.A., 2008. The effect of respiration variations on independent component analysis results of resting state functional connectivity. Hum. Brain Mapp. 29, 740–750.
Biswal, B., Yetkin, F.Z., Haughton, V.M., Hyde, J.S., 1995. Functional connectivity in the motor cortex of resting human brain using echo-planar MRI. Magn. Reson. Med. 34, 537–541.
Biswal, B., Hudetz, A.G., Yetkin, F.Z., Haughton, V.M., Hyde, J.S., 1997. Hypercapnia reversibly suppresses low-frequency fluctuations in the human motor cortex during rest using echo-planar MRI. J. Cereb. Blood Flow Metab. 17, 301–308.
Bland, J.M., Altman, D.G., 1996. Measurement error and correlation coefficients. BMJ 313, 41–42.
Broyd, S.J., Demanuele, C., Debener, S., Helps, S.K., James, C.J., Sonuga-Barke, E.J., 2009. Default-mode brain dysfunction in mental disorders: a systematic review. Neurosci. Biobehav. Rev. 33, 279–296.
Buckner, R.L., Vincent, J.L., 2007. Unrest at rest: default activity and spontaneous network correlations. Neuroimage 37, 1091–1096 discussion 1097-1099..
Bullmore, E., Fadili, J., Maxim, V., Sendur, L., Whitcher, B., Suckling, J., Brammer, M., Breakspear, M., 2004. Wavelets and functional magnetic resonance imaging of the human brain. Neuroimage 23 (Suppl. 1), S234–249.
Bush, G., Valera, E.M., Seidman, L.J., 2005. Functional neuroimaging of attention-deficit/hyperactivity disorder: a review and suggested future directions. Biol. Psychiatry 57, 1273–1284.
Buzsáki, G., Draguhn, A., 2004. Neuronal oscillations in cortical networks. Science 304, 1926–1929.
Castellanos, F.X., Tannock, R., 2002. Neuroscience of attention-deficit/hyperactivity disorder: the search for endophenotypes. Nat. Rev. Neurosci. 3, 617–628.
Chang, C., Cunningham, J.P., Glover, G.H., 2009. Influence of heart rate on the BOLD signal: the cardiac response function. Neuroimage 44, 857–869.
Chen, G., Popa, L.S., Wang, X., Gao, W., Barnes, J., Hendrix, C.M., Hess, E.J., Ebner, T.J., 2009. Low-frequency oscillations in the cerebellar cortex of the tottering mouse. J. Neurophysiol. 101, 234–245.
Cordes, D., Haughton, V.M., Arfanakis, K., Carew, J.D., Turski, P.A., Moritz, C.H., Quigley, M.A., Meyerand, M.E., 2001. Frequencies contributing to functional connectivity in the cerebral cortex in "resting-state" data. AJNR Am. J. Neuroradiol. 22, 1326–1333.
Dagli, M.S., Ingeholm, J.E., Haxby, J.V., 1999. Localization of cardiac-induced signal change in fMRI. Neuroimage 9, 407–415.
De Luca, M., Beckmann, C.F., De Stefano, N., Matthews, P.M., Smith, S.M., 2006. fMRI resting state networks define distinct modes of long-distance interactions in the human brain. Neuroimage 29, 1359–1367.
Demanuele, C., James, C.J., Sonuga-Barke, E.J., 2007. Distinguishing low frequency oscillations within the 1/f spectral behaviour of electromagnetic brain signals. Behav. Brain Funct. 3, 62.
Deuker, L., Bullmore, E.T., Smith, M., Christensen, S., Nathan, P.J., Rockstroh, B., Bassett, D.S., 2009. Reproducibility of graph metrics of human brain functional networks. Neuroimage 47, 1460–1468.
Di Martino, A., Ghaffari, M., Curchack, J., Reiss, P., Hyde, C., Vannucci, M., Petkova, E., Klein, D.F., Castellanos, F.X., 2008a. Decomposing intra-subject variability in children with attention-deficit/hyperactivity disorder. Biol. Psychiatry 64, 607–614.

Di Martino, A., Scheres, A., Margulies, D.S., Kelly, A.M., Uddin, L.Q., Shehzad, Z., Biswal, B., Walters, J.R., Castellanos, F.X., Milham, M.P., 2008b. Functional connectivity of human striatum: a resting state FMRI study. Cereb. Cortex 18, 2735–2747.
Di Martino, A., Shehzad, Z., Kelly, A.M.C., Roy Krain, A., Gee, D., Uddin, L., Gotimer, K., Klein, D.F., Castellanos, F.X., Milham, M.P., 2009. Relationship between cingulo-insular functional connectivity and autistic traits in neurotypical adults. Am. J. of. Psychiatry 166, 891–899.
Duff, E.P., Johnston, L.A., Xiong, J., Fox, P.T., Mareels, I., Egan, G.F., 2008. The power of spectral density analysis for mapping endogenous BOLD signal fluctuations. Hum. Brain Mapp. 29, 778–790.
Fox, M.D., Raichle, M.E., 2007. Spontaneous fluctuations in brain activity observed with functional magnetic resonance imaging. Nat. Rev. Neurosci. 8, 700–711.
Fox, M.D., Snyder, A.Z., Vincent, J.L., Raichle, M.E., 2007. Intrinsic fluctuations within cortical systems account for intertrial variability in human behavior. Neuron 56, 171–184.
Fox, M.D., Zhang, D., Snyder, A.Z., Raichle, M.E., 2009. The global signal and observed anticorrelated resting state brain networks. J. Neurophysiol. 101, 3270–3283.
Fransson, P., 2006. How default is the default mode of brain function? Further evidence from intrinsic BOLD signal fluctuations. Neuropsychologia 44, 2836–2845.
Fukunaga, M., Horovitz, S.G., de Zwart, J.A., van Gelderen, P., Balkin, T.J., Braun, A.R., Duyn, J.H., 2008. Metabolic origin of BOLD signal fluctuations in the absence of stimuli. J. Cereb. Blood Flow Metab. 28, 1377–1387.
Ghosh, A., Rho, Y., McIntosh, A.R., Kotter, R., Jirsa, V.K., 2008. Noise during rest enables the exploration of the brain's dynamic repertoire. PLoS Comput. Biol. 4, e1000196.
Greicius, M., 2008. Resting-state functional connectivity in neuropsychiatric disorders. Curr. Opin. Neurol. 21, 424–430.
Greicius, M.D., Supekar, K., Menon, V., Dougherty, R.F., 2009. Resting-state functional connectivity reflects structural connectivity in the default mode network. Cereb. Cortex 19, 72–78.
Gusnard, D.A., Raichle, M.E., 2001. Searching for a baseline: functional imaging and the resting human brain. Nat. Rev. Neurosci. 2, 685–694.
Hagmann, P., Cammoun, L., Gigandet, X., Meuli, R., Honey, C.J., Wedeen, V.J., Sporns, O., 2008. Mapping the structural core of human cerebral cortex. PLoS Biol. e159, 6.
Hampson, M., Driesen, N.R., Skudlarski, P., Gore, J.C., Constable, R.T., 2006. Brain connectivity related to working memory performance. J. Neurosci. 26, 13338–13343.
He, B.J., Snyder, A.Z., Zempel, J.M., Smyth, M.D., Raichle, M.E., 2008. Electrophysiological correlates of the brain's intrinsic large-scale functional architecture. Proc. Natl. Acad. Sci. U. S. A. 105, 16039–16044.
He, Y., Wang, J., Wang, L., Chen, Z.J., Yan, C., Yang, H., Tang, H., Zhu, C., Gong, Q., Zang, Y., Evans, A.C., 2009. Uncovering intrinsic modular organization of spontaneous brain activity in humans. PLoS ONE 4, e5226.
Hesselmann, G., Kell, C.A., Eger, E., Kleinschmidt, A., 2008. Spontaneous local variations in ongoing neural activity bias perceptual decisions. Proc. Natl. Acad. Sci. U. S. A. 105, 10984–10989.
Honey, C.J., Sporns, O., Cammoun, L., Gigandet, X., Thiran, J.P., Meuli, R., Hagmann, P., 2009. Predicting human resting-state functional connectivity from structural connectivity. Proc. Natl. Acad. Sci. U. S. A. 106, 2035–2040.
Horovitz, S.G., Fukunaga, M., de Zwart, J.A., van Gelderen, P., Fulton, S.C., Balkin, T.J., Duyn, J.H., 2008. Low frequency BOLD fluctuations during resting wakefulness and light sleep: a simultaneous EEG-fMRI study. Hum. Brain Mapp. 29, 671–682.
Hutchison, W.D., Dostrovsky, J.O., Walters, J.R., Courtemanche, R., Boraud, T., Goldberg, J., Brown, P., 2004. Neuronal oscillations in the basal ganglia and movement disorders: evidence from whole animal and human recordings. J. Neurosci. 24, 9240–9243.
Jezzard, P., LeBihan, D., Cuenod, C., Pannier, L., Prinster, A., Turner, R., 1993. An investigation of the contribution of physiological noise in human functional MRI studies at 1.5 Tesla and 4 Tesla. Proceedings of the 12th Annual Meeting of SMRM, New York, p. 1392.
Julien, C., 2006. The enigma of Mayer waves: Facts and models. Cardiovasc. Res. 70, 12–21.
Kannurpatti, S.S., Biswal, B.B., 2008. Detection and scaling of task-induced fMRI-BOLD response using resting state fluctuations. Neuroimage 40, 1567–1574.
Kelly, A.M., Uddin, L.Q., Biswal, B.B., Castellanos, F.X., Milham, M.P., 2008. Competition between functional brain networks mediates behavioral variability. Neuroimage 39, 527–537.
Kennedy, D.N., Lange, N., Makris, N., Bates, J., Meyer, J., Caviness Jr, V.S., 1998. Gyri of the human neocortex: an MRI-based analysis of volume and variance. Cereb. Cortex 8, 372–384.
Kiviniemi, V., Jauhiainen, J., Tervonen, O., Paakko, E., Oikarinen, J., Vainionpaa, V., Rantala, H., Biswal, B., 2000. Slow vasomotor fluctuation in fMRI of anesthetized child brain. Magn. Reson. Med. 44, 373–378.
Kiviniemi, V., Kantola, J.H., Jauhiainen, J., Hyvarinen, A., Tervonen, O., 2003. Independent component analysis of nondeterministic fMRI signal sources. Neuroimage 19, 253–260.
Kiviniemi, V.J., Haanpaa, H., Kantola, J.H., Jauhiainen, J., Vainionpaa, V., Alahuhta, S., Tervonen, O., 2005. Midazolam sedation increases fluctuation and synchrony of the resting brain BOLD signal. Magn. Reson. Imaging 23, 531–537.
Knyazev, G.G., 2007. Motivation, emotion, and their inhibitory control mirrored in brain oscillations. Neurosci. Biobehav. Rev. 31, 377–395.
Legendre, P., 2005. Species associations: The Kendall coefficient of concordance revisited. J. Agric. Biol. Environ. Stat. 10, 226–245.
Leopold, D.A., Murayama, Y., Logothetis, N.K., 2003. Very slow activity fluctuations in monkey visual cortex: implications for functional brain imaging. Cereb. Cortex 13, 422–433.
Lu, H., Zuo, Y., Gu, H., Waltz, J.A., Zhan, W., Scholl, C.A., Rea, W., Yang, Y., Stein, E.A., 2007. Synchronized delta oscillations correlate with the resting-state functional MRI signal. Proc. Natl. Acad. Sci. U. S. A. 104, 18265–18269.
Makris, N., Meyer, J.W., Bates, J.F., Yeterian, E.H., Kennedy, D.N., Caviness, V.S., 1999. MRI-Based topographic parcellation of human cerebral white matter and nuclei: II. Rationale and applications with systematics of cerebral connectivity. Neuroimage 9, 18–45.
Mantini, D., Perrucci, M.G., Del Gratta, C., Romani, G.L., Corbetta, M., 2007. Electrophysiological signatures of resting state networks in the human brain. Proc. Natl. Acad. Sci. U. S. A. 104, 13170–13175.
Margulies, D.S., Kelly, A.M., Uddin, L.Q., Biswal, B.B., Castellanos, F.X., Milham, M.P., 2007. Mapping the functional connectivity of anterior cingulate cortex. Neuroimage 37, 579–588.
Maxim, V., Sendur, L., Fadili, J., Suckling, J., Gould, R., Howard, R., Bullmore, E., 2005. Fractional Gaussian noise, functional MRI and Alzheimer's disease. Neuroimage 25, 141–158.
McAvoy, M., Larson-Prior, L., Nolan, T.S., Vaishnavi, S.N., Raichle, M.E., d'Avossa, G., 2008. Resting states affect spontaneous BOLD oscillations in sensory and paralimbic cortex. J. Neurophysiol. 100, 922–931.
Monto, S., Palva, S., Voipio, J., Palva, J.M., 2008. Very slow EEG fluctuations predict the dynamics of stimulus detection and oscillation amplitudes in humans. J. Neurosci. 28, 8268–8272.
Murphy, K., Birn, R.M., Handwerker, D.A., Jones, T.B., Bandettini, P.A., 2009. The impact of global signal regression on resting state correlations: are anti-correlated networks introduced? Neuroimage 44, 893–905.
Penttonen, M., 2003. Natural logarithmic relationship between brain oscillators. Thalamus and Related Systems 2, 145–152.
Petridou, N., Schäfer, A., Gowland, P., Bowtell, R., 2009. Phase vs. magnitude information in functional magnetic resonance imaging time series: toward understanding the noise. Magn. Reson. Imaging. 27, 1046–1057.
Picchioni, D., Fukunaga, M., Carr, W.S., Braun, A.R., Balkin, T.J., Duyn, J.H., Horovitz, S.G., 2008. fMRI differences between early and late stage-1 sleep. Neurosci. Lett. 441, 81–85.
Raichle, M.E., 2009. A brief history of human brain mapping. Trends Neurosci. 32, 118–126.
Raichle, M.E., Mintun, M.A., 2006. Brain work and brain imaging. Annu. Rev. Neurosci. 29, 449–476.
Raichle, M.E., MacLeod, A.M., Snyder, A.Z., Powers, W.J., Gusnard, D.A., Shulman, G.L., 2001. A default mode of brain function. Proc. Natl. Acad. Sci. U. S. A. 98, 676–682.
Ruskin, D.N., Bergstrom, D.A., Kaneoke, Y., Patel, B.N., Twery, M.J., Walters, J.R., 1999a. Multisecond oscillations in firing rate in the basal ganglia: robust modulation by dopamine receptor activation and anesthesia. J. Neurophysiol. 81, 2046–2055.
Ruskin, D.N., Bergstrom, D.A., Mastropietro, C.W., Twery, M.J., Walters, J.R., 1999b. Dopamine agonist-mediated rotation in rats with unilateral nigrostriatal lesions is not dependent on net inhibitions of rate in basal ganglia output nuclei. Neuroscience 91, 935–946.
Ruskin, D.N., Bergstrom, D.A., Shenker, A., Freeman, L.E., Baek, D., Walters, J.R., 2001. Drugs used in the treatment of attention-deficit/hyperactivity disorder affect postsynaptic firing rate and oscillation without preferential dopamine autoreceptor action. Biol. Psychiatry 49, 340–350.
Salvador, R., Achard, S., Bullmore, E., 2007. Frequency-Dependent Functional Connectivity Analysis of fMRI Data in Fourier and Wavelet Domains. Handbook of Brain Connectivity. Springer, Berlin / Heidelberg, pp. 379–401.
Salvador, R., Martinez, A., Pomarol-Clotet, E., Gomar, J., Vila, F., Sarro, S., Capdevila, A., Bullmore, E., 2008. A simple view of the brain through a frequency-specific functional connectivity measure. Neuroimage 39, 279–289.
Seeley, W.W., Crawford, R.K., Zhou, J., Miller, B.L., Greicius, M.D., 2009. Neurodegenerative diseases target large-scale human brain networks. Neuron 62, 42–52.
Shehzad, Z., Kelly, A.M., Reiss, P.T., Gee, D.G., Gotimer, K., Uddin, L.Q., Lee, S.H., Margulies, D.S., Roy, A.K., Biswal, B.B., Petkova, E., Castellanos, F.X., Milham, M.P., 2009. The Resting Brain: Unconstrained yet Reliable. Cereb. Cortex 19, 2209–2229.
Shmueli, K., van Gelderen, P., de Zwart, J.A., Horovitz, S.G., Fukunaga, M., Jansma, J.M., Duyn, J.H., 2007. Low-frequency fluctuations in the cardiac rate as a source of variance in the resting-state fMRI BOLD signal. Neuroimage 38, 306–320.
Shrout, P.E., Fleiss, J.L., 1979. Intraclass correlations: uses in assessing rater reliability. Psychol. Bull. 86, 420–428.
Suckling, J., Wink, A.M., Bernard, F.A., Barnes, A., Bullmore, E., 2008. Endogenous multifractal brain dynamics are modulated by age, cholinergic blockade and cognitive performance. J. Neurosci. Methods 174, 292–300.
Uitert, G.C.V., 1978. Reduction of leakage and increase of resolution in power spectral density and coherence functions. Nucl. Instrum. Methods 157, 583–589.
van Buuren, M., Gladwin, T.E., Zandbelt, B.B., van den Heuvel, M., Ramsey, N.F., Kahn, R.S., Vink, M., 2009. Cardiorespiratory effects on default-mode network activity as measured with fMRI. Hum. Brain. Mapp. 30, 3031–3042.
van den Heuvel, M.P., Mandl, R.C., Kahn, R.S., Hulshoff Pol, H.E., 2009. Functionally linked resting-state networks reflect the underlying structural connectivity architecture of the human brain. Hum. Brain. Mapp. 30, 3127–3141.
van Vugt, M.K., Sederberg, P.B., Kahana, M.J., 2007. Comparison of spectral analysis methods for characterizing brain oscillations. J. Neurosci. Methods 162, 49–63.
Vanhatalo, S., Palva, J.M., Holmes, M.D., Miller, J.W., Voipio, J., Kaila, K., 2004. Infraslow oscillations modulate excitability and interictal epileptic activity in the human cortex during sleep. Proc. Natl. Acad. Sci. U. S. A. 101, 5053–5057.
Warner, R.M., 1998. Spectral Analysis of Time-Series Data. The Guilford Press, New York.
Wink, A.M., Bullmore, E., Barnes, A., Bernard, F., Suckling, J., 2008. Monofractal and multifractal dynamics of low frequency endogenous brain oscillations in functional MRI. Hum. Brain Mapp. 29, 791–801.
Wise, R.G., Ide, K., Poulin, M.J., Tracey, I., 2004. Resting fluctuations in arterial carbon dioxide induce significant low frequency variations in BOLD signal. Neuroimage 21, 1652–1664.
Yamazaki, K., Uchida, M., Obata, A., Katura, T., Sato, H., Tanaka, N., Maki, A., 2007. Comparison between Spontaneous Low-Frequency Oscillations in Regional Cerebral Blood Volume, and Cerebral and Plethysmographic Pulsations. NOISE AND FLUCTUATIONS: 19th International Conference on Noise and Fluctuations; ICNF 2007. AIP Conference Proceedings, pp. 687–690.

Yan, L., Zhuo, Y., Ye, Y., Xie, S.X., An, J., Aguirre, G.K., Wang, J., 2009. Physiological origin of low-frequency drift in blood oxygen level dependent (BOLD) functional magnetic resonance imaging (fMRI). Magn. Reson. Med. 61, 819–827.

Yang, H., Long, X.Y., Yang, Y., Yan, H., Zhu, C.Z., Zhou, X.P., Zang, Y.F., Gong, Q.Y., 2007. Amplitude of low frequency fluctuation within visual areas revealed by resting-state functional MRI. Neuroimage 36, 144–152.

Zang, Y.F., He, Y., Zhu, C.Z., Cao, Q.J., Sui, M.Q., Liang, M., Tian, L.X., Jiang, T.Z., Wang, Y.F., 2007. Altered baseline brain activity in children with ADHD revealed by resting-state functional MRI. Brain Dev. 29, 83–91.

Zhang, Z.Q., Lu, G.M., Zhong, Y., Tan, Q.F., Zhu, J.G., Jiang, L., Chen, Z.L., Wang, Z.Q., Shi, J. X., Zang, Y.F., Liu, Y.J., 2008. [Application of amplitude of low-frequency fluctuation to the temporal lobe epilepsy with bilateral hippocampal sclerosis: an fMRI study]. Zhonghua Yi Xue Za Zhi 88, 1594–1598.

Zou, Q.H., Zhu, C.Z., Yang, Y., Zuo, X.N., Long, X.Y., Cao, Q.J., Wang, Y.F., Zang, Y.F., 2008. An improved approach to detection of amplitude of low-frequency fluctuation (ALFF) for resting-state fMRI: fractional ALFF. J. Neurosci. Methods 172, 137–141.

Zou, Q., Wu, C.W., Stein, E.A., Zang, Y., Yang, Y., 2009. Static and dynamic characteristics of cerebral blood flow during the resting state. Neuroimage 48, 515–524.